Metals and Materials International
https://doi.org/10.1007/s12540-024-01715-8

Thermodynamic and Kinetic Analysis of Non-Metallic Inclusions Evolution in Si-Killed 316L Stainless Steel with Various Refining Slags

Shengchao Duan[1,2] · Taesung Kim[3] · Jinhyung Cho[3] · Joo Hyun Park[2]

Received: 18 December 2023 / Accepted: 5 May 2024

Abstract
Reactions between Si-killed 316L stainless steel (STS316L) and CaO–SiO_2–CaF_2–5%MgO–5%Al_2O_3 slag were conducted in a magnisa crucible at 1873 K to study the influences of slag binary basicity (CaO/SiO_2) ratio and CaF_2 content on the formation of inclusions in molten steel. Increasing the binary basicity from C/S = 1.0 to 2.3 while keeping CaF_2 content constant at 10 wt% led to a significant decrease in the total oxygen content in the molten steel. However, changing the CaF_2 content from 10 to 30 wt% had minimal impact on reducing the total oxygen content (at C/S = 1.7). The transformation of inclusions from initial SiO_2 and MnO–Cr_2O_3 inclusions to MgO·Al_2O_3 spinel phases and pure MgO particles occurred in the molten Si-killed STS316L when the slag had basicity values of C/S = 1.7 and 2.3, respectively. In this scenario, Al_2O_3 inclusion could serve as an intermediary product during the mentioned transformation process. However, the utilization of slags with lower basicity (C/S = 1.0–1.3) led to the occurrence of liquid inclusions instead. The presence of Al_2O_3 inclusions in the molten steel can be linked to the higher Al_2O_3 activity in extremely basic slag compositions. Furthermore, the activity of MgO in high basicity and low viscosity slags (C/S = 1.7–2.3) is nearly equal to unity, causing the transfer of Mg from the slag and subsequently resulting in the transformation of inclusions from Al_2O_3 to MgO·Al_2O_3 and MgO inclusions under slag basicity values of 1.7 and 2.3, correspondingly, at a temperature of 1873 K.

Keywords 316L stainless steel · Slag · Inclusion · Basicity · Spinel · Viscosity

1 Introduction

316L austenitic stainless steel (STS316L) is a widely used material in various industries, such as aerospace, marine, and nuclear sectors [1–4], due to its outstanding formability and excellent resistance to corrosion [5, 6], as well as oxidation [7–9]. However, nonmetallic inclusions (NMIs) are formed unavoidably during the steelmaking process [10]. Failure to correctly and efficiently regulate the morphology, composition, and particle size distribution of NMI can adversely influence the manufacturing process and impair the mechanical characteristics of steel products [11]. Therefore, monitoring the formation and evolution of NMIs throughout the STS316L production process is crucial.

Anable et al. [12] studied the impact of CaF_2–CaO–Al_2O_3–MgO slag composition on the electroslag remelting (ESR) of STS316L. They noted that remelted ingots had elevated residual Al levels (> 0.05 wt%) due to the higher Al_2O_3 content (> 20 wt%) in the ESR type slag, with oxygen content increasing from around 30 to 100 ppm after alternating current ESR. Eo et al. [13] utilized laser metal deposition to investigate inclusion evolution in the additive manufacture of STS316L, observing that oxygen content and inclusion density ranged from approximately 300 to 1000 ppm and 17,000 to 34,000 per mm^2, respectively. The faster cooling rate led to smaller inclusions being more evenly dispersed, consequently enhancing the tensile yield stress of steel. Vukkum and Gupta [14] conducted a review of the corrosion characteristics of STS316L fabricated using the laser powder bed fusion (LPBF) printing method. They found that the chemical compositions of precipitated inclusions in LPBF-316L steel differed from previous studies [15–20], while the corrosion resistance of LPBF-316L was

✉ Joo Hyun Park
basicity@hanyang.ac.kr

1 School of Mechanical and Materials Engineering, North China University of Technology, Beijing 100144, China

2 Department of Materials Science and Chemical Engineering, Hanyang University, Ansan 15588, Republic of Korea

3 Research and Development Center, Hyundai Steel, Dangjin 31719, Republic of Korea

Published online: 06 June 2024

enhanced by regulating inclusion compositions according to their intended application.

The ladle furnace (LF) is a well-established technology commonly employed in the secondary refining of steel [21]. This process involves modifying and ensuring uniformity in the steel composition, along with eliminating non-metallic inclusions (NMI), through techniques such as steel reheating and argon stirring [22–24]. In a study by Sakata [25], a refining method was developed for the efficient casting of STS304 and STS316L stainless steels. It was discovered that effective regulation of oxygen content in the LF refining process is achievable under optimal conditions, including treatment duration, bottom bubbling gas flow rate, and slag composition.

Yin et al. [26] and Park [27] analyzed data from the industrial trials (AOD → LF → CC process) to investigate the characteristics of inclusions in austenitic stainless steels. Their findings revealed that the Al_2O_3 and MgO contents of the inclusions in the steel increased gradually from the AOD stage to the CC stage. It has been emphasized that the composition of ladle slag plays a crucial role in eliminating inclusions and enhancing the cleanliness of stainless steel [28–33]. Shin and Park conducted research on the reactions between $CaO–Al_2O_3–SiO_2–MgO–CaF_2$ ladle slag with varying CaO/Al_2O_3 ratios and a Fe–0.4C–0.7Si–1.4Mn–0.2 V (wt%) alloy in an induction furnace at 1873 K [32]. Their study revealed that maintaining the C/A ratio in the range of 1.5 and 2.5 in the slag effectively suppressed the generation of harmful solid spinel and MgO inclusions in the alloy. Guo et al. [33] optimized the basicity of ladle slag to achieve a balance between enhancing NMI plasticity and improving the cleanliness of STS304. Their research indicated that maintaining the slag basicity within the range of C/S = 1.4 to 1.8 and the soluble Al content in the steel below 10 ppm led to favorable inclusion plasticity and relatively high steel cleanliness based on the results of both laboratory experiments and industrial trials.

Silicon is commonly employed as the deoxidizer in refining STS316L instead of aluminum because the deoxidation products typically form liquid silicates that solidify into a spherical shape when casting slabs or blooms [26, 34]. In a recent study by Zhang et al. [35], they investigated how the ratios of C/S and C/A in the $CaO–SiO_2–Al_2O_3–MgO$ slag affect the removal and transformation of inclusions in STS430. It was observed that increasing the basicity from C/S = 1.0 to 5.0 resulted in a decrease in total oxygen content from around 70 to 40 ppm while adjusting the C/A ratio had minimal impact on the cleanliness of the steel.

Based on these findings, more study is needed to determine how the binary basicity (CaO/SiO_2) and CaF_2 concentration of the $CaO–SiO_2–CaF_2–5\%Al_2O_3–5\%MgO$ ladle slag influence the evolution of inclusions and the deoxidation process in Si-killed STS316L. Therefore, the aim of this study is to experimentally and theoretically investigate the interactions between the ladle slag, STS316L, and MgO refractory and further to illustrate the evolution mechanism of inclusions during the LF refining processes. A detailed explanation of the modeling and calculation procedures of the thermodynamic model used in this study can be found in previous publications [36–39].

2 Experimental Procedure

The experiments involving ladle slag (60 g) and Si-killed STS316L (600 g) were conducted using a high-frequency induction furnace equipped with a magnisa crucible, as depicted in Fig. 1. After reaching the pre-set temperature of 1873 K, the furnace introduced pure silicon, acting as a deoxidizer, into the molten steel under an inert atmosphere to regulate the silicon content to 0.4 wt%. The initial chemical composition of STS316L prior to deoxidation is outlined in Table 1. The steel was maintained at this temperature for 30 min after silicon deoxidation to ensure a uniform composition.

High-grade powders of SiO_2, Al_2O_3, MgO, and CaF_2 were employed as raw materials. Calcium oxide (CaO) was ontained by heating reagent-grade $CaCO_3$ at 1273 K in a muffle furnace. For thorough fusion, these powders were appropriately mixed and melted in a graphite crucible at 1873 K under a high-purity Ar atmosphere. The chemical compositions of the ladle slag can be found in Table 2 and represented in Fig. 2. The Vee ratio (CaO/SiO_2 = C/S) and CaF_2 content of the slag varied from C/S = 1.0 to 2.3 and from 10 to 30 wt%, respectively.

At first, a metal sample was taken with a quartz sampler before adding the ladle slag. Then, 60 g of ladle slag were quickly placed onto the surface of the molten steel. The commencement of the reaction was identified as the point when the molten slag made contact with the steel. Steel and slag samples were promptly taken from the crucible at set time intervals (5, 10, 30, and 60 min) during the reaction and rapidly cooled by immersing them in brine. The detail of the experimental operation procedure and the analysis methods for the measurements of total oxygen content (T.[O]) and characterizations of inclusion in the STS316L has been described elsewhere [40].

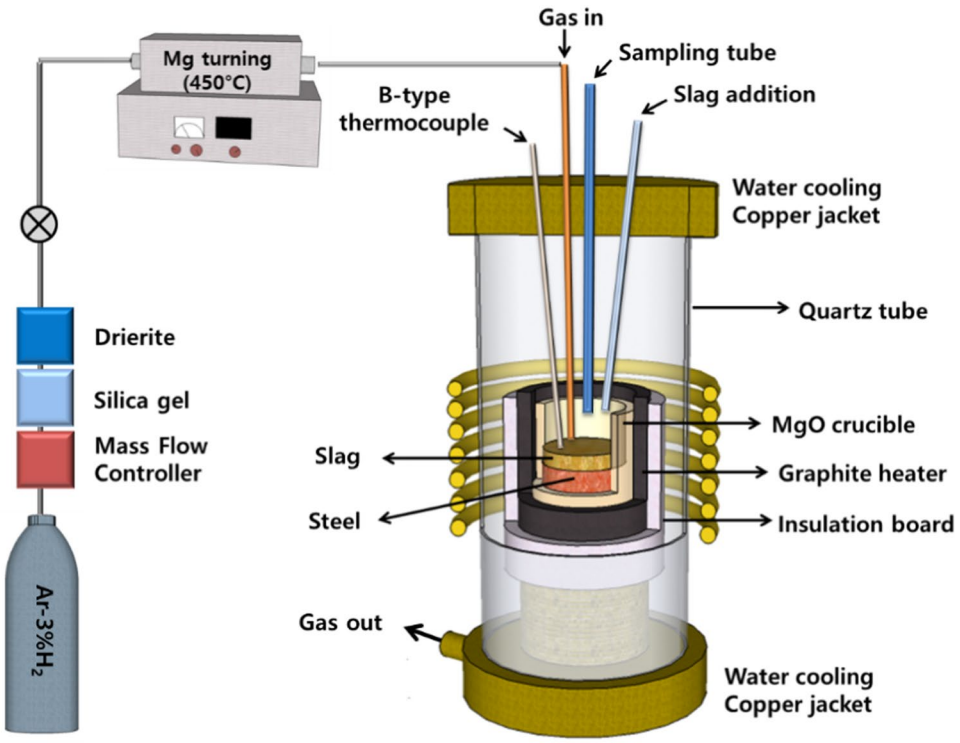

Fig. 1 Illustration of the experimental equipment

Table 1 Chemical composition of STS316L before deoxidation (wt%)

C	Si	Mn	Cu	Ni	Cr	Mo	O	S	Fe
0.005	0.03	0.5	0.3	12.3	16.2	2.1	0.009	0.03	Bal

Table 2 Chemical composition of ladle slag used in the present study (wt%)

Variables	Slag No	CaO	SiO_2	Al_2O_3	MgO	CaF_2	C/S
	S1	40.0	40.0	5.0	5.0	10.0	1.0
	S2	48.0	32.0	5.0	5.0	10.0	1.3
CaO/SiO_2 ratio	S3	50.3	29.6	5.0	5.0	10.0	1.7
	S4	56.0	24.0	5.0	5.0	10.0	2.3
	S5	47.2	27.8	5.0	5.0	15.0	1.7
CaF_2 content	S6	44.0	25.8	5.0	5.0	20.0	1.7
	S7	40.9	24.1	5.0	5.0	25.0	1.7
	S8	37.8	22.2	5.0	5.0	30.0	1.7

3 Results and Discussion

3.1 Effect of Slag Composition on the Deoxidation Behavior of Si-Killed STS316L

The graph in Fig. 3 demonstrates the variations in total oxygen content (T.[O]) in liquid STS316L over reaction time at 1873 K, with varying Vee ratio (C/S) and CaF_2 levels in the ladle slag. The T.[O] in the liquid steel decreases notably as the reaction time increases up to 30 min at the given Vee ratio (Fig. 3a) followed by stabilization, indicating that the deoxidation reaction reaches chemical equilibrium at 1873 K. Additionally, there is a significant reduction in T.[O] in the liquid steel when the Vee ratio changes from C/S = 1.0 to 1.7 within 10 min, with the effect leveling off between C/S = 1.7 to 2.3. Previous studies [31, 41–45] have also reported a similar trend.

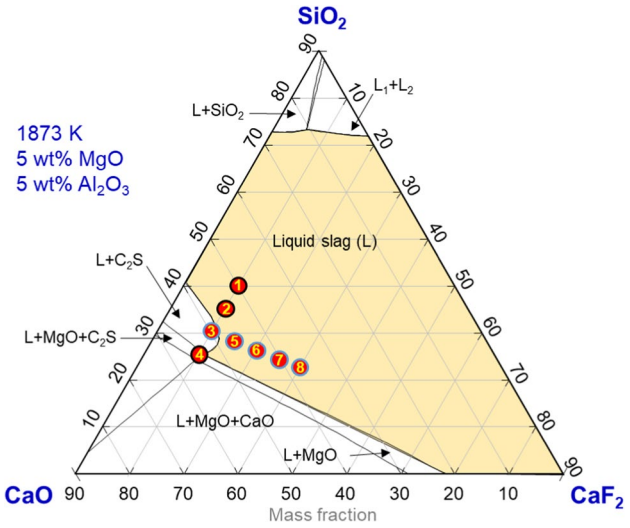

Fig. 2 Phase diagram of slag used in the present study at 1873 K

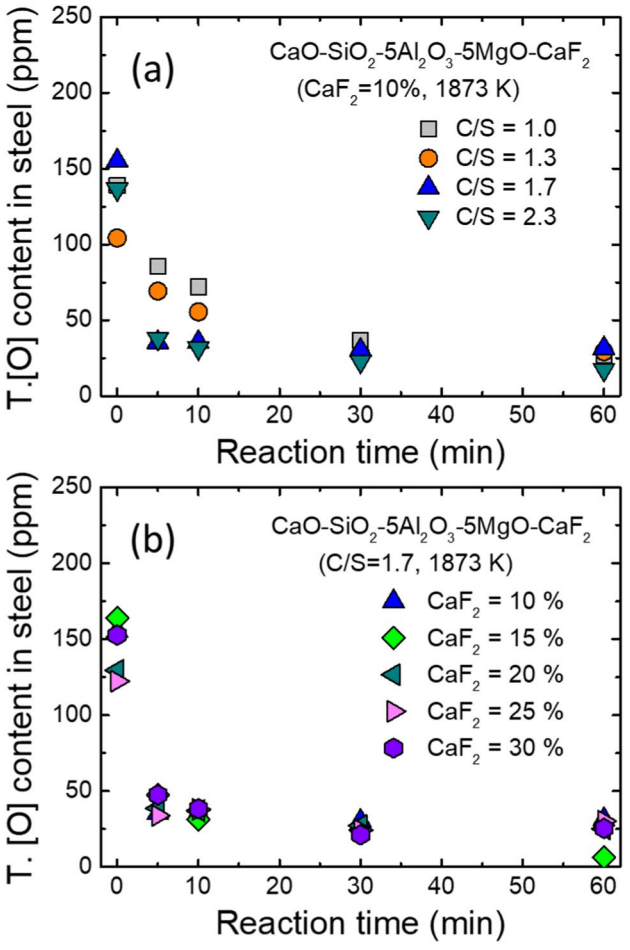

Fig. 3 Effects on the T.[O] in the steel at 1873 K of (**a**) binary basicity (CaO/SiO_2) and (**b**) CaF_2 concentration in the $CaO–SiO_2–CaF_2–5\%MgO–5\%Al_2O_3$ slag

The impact of different concentrations of CaF_2 in slag on the fluctuation of total oxygen levels in molten steel is shown in Fig. 3b. At 1873 K with a constant Vee ratio C/S = 1.7, the amount of CaF_2 has little effect on reducing the total oxygen in the liquid steel. These results suggest that changes in the basicity of ladle slag have a more pronounced influence on the total oxygen levels in molten steel compared to the CaF_2 concentration at this temperature. In their plant trials, Andersson et al. [46] found that the presence of CaF_2 had minimal impact on the quantity and types of inclusions in steel refining. Similarly, Zheng et al. [47] found that the refining capability of $CaO–SiO_2–MgO–Al_2O_3–TiO_2–CaF_2$ slag for producing Al-killed duplex stainless steel was not significantly influenced by the CaF_2 concertration.

Assuming the total oxygen removal reaction is a first-order reaction [30], the change of total oxygen content with reaction time in the liquid steel can be formulated as Eqs. (1) and (2).

$$-\frac{d[\%O]_t}{dt} = k_{App.}\left([\%O]_t - [\%O]_e\right) \tag{1}$$

$$-\ln\left(\frac{[\%\,O]_t - [\%\,O]_e}{[\%\,O]_o - [\%\,O]_e}\right) = k_{App.}t \tag{2}$$

where, $[\%O]_t$, $[\%O]_e$, and $[\%O]_o$ stand for the total oxygen content in the melt at arbitrary reaction time t, the total oxygen content at the equilibrium state, and the initial total oxygen content in the melt, respectively. $k_{App.}$ is an apparent rate constant of oxygen removal reaction. Effects of various basicity (C/S) and CaF_2 contents in the ladle slag on the $k_{App.}$ are illustrated in Fig. 4, which shows that the relationships between the apparent rate constant $k_{App.}$ and basicity as well as CaF_2 content under the present experimental conditions are consistent with all the previously mentioned observations displayed in Fig. 3.

The rise in the value of $k_{App.}$ resulting from the escalation in slag basicity is attributed to the accelerated dissolution rate of non-metallic inclusions (NMI) into the slag. High-basicity slag notably reduces the overall dissolution duration of NMIs. According to Valdez et al. [48], the relationship between total dissolution time of NMI (τ) into the slag and physcochemical properties of slag was given in Eq. (3).

$$\tau \propto \frac{\eta}{\Delta C} \tag{3}$$

where, η is the slag viscosity; the concentration difference (the force that accelerates inclusion dissolution into slag) can be expressed as ΔC. Equation (3) makes it evident that there is a positive relation between the total dissolution time of inclusion (τ) and the ratio of the viscosity η and ΔC.

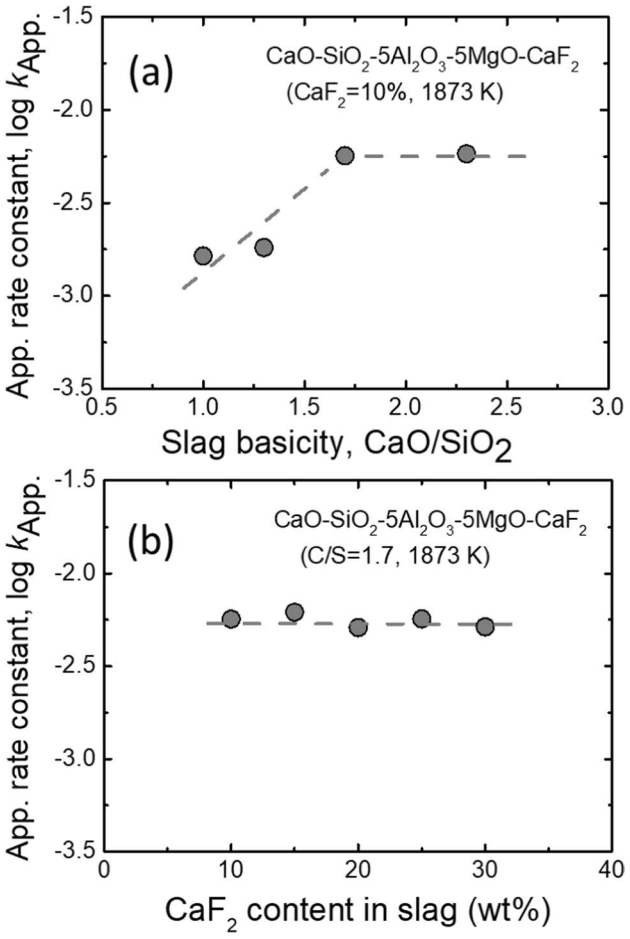

Fig. 4 Effects on the apparent rate constant $k_{App.}$ of the oxygen removal reaction at 1873 K of (**a**) binary basicity and (**b**) CaF_2 concentration in the $CaO–SiO_2–CaF_2–5\%MgO–5\%Al_2O_3$ slag

In their study, Gao et al. [49] explored the impact of slag basicity (C/S) on the viscosity of $CaO–SiO_2–MgO–Al_2O_3$ slag through the rotating cylinder method. Their findings revealed that as slag basicity increased, the complex aluminosilicate network structure of the slag underwent depolymerization into simpler units. Consequently, this led to a decrease in slag viscosity with higher slag basicity. Deng et al. [50], Jeong et al. [51], and Han et al. [52] also noted that the viscosity and melting temperature of $CaO–Al_2O_3–MgO–SiO_2–CaF_2$ slag decreased with higher amounts of CaF_2. Park et al. [53] introduced the iso-viscosity contour in the $CaO–SiO_2–CaF_2$ system at 1873 K, observing a similar trend where the viscosity of the silicate system in the relatively acidic region ($C/S < 1.0$) decreased with an increased CaF_2 content, but remained relatively unaffected by CaF_2 in the relatively basic region ($C/S > 1.5$).

Zhang and Chou [54] developed a model at 1873 K to predict the viscosity of $CaO–SiO_2–CaF_2$ slag melts. They determined that replacing CaO with CaF_2 in the slag leads to a decrease in viscosity in low basicity conditions, while viscosity remains nearly constant in high basicity conditions at 1873 K. Park et al. [55] used FT-IR spectroscopy to examine the structures of $CaO–SiO_2$ and $CaO–SiO_2–CaF_2$ slags. Their analysis revealed that as the C/S ratio increased, the viscosities of the $CaO–SiO_2$ and $CaO–SiO_2–CaF_2$ slags decreased due to a rise in non-bridging oxygen per silicon (NBO/Si) with the C/S ratio. Additionally, the introduction of CaF_2 into the high basicity slag system ($C/S > 1.5$) did not significantly alter the NBO/Si ratio.

Hence, an increase in slag basicity can reduce the viscosity of the $CaO–SiO_2–CaF_2–5\%MgO–5\%Al_2O_3$ slag while also enhancing the concentration difference ΔC. This leads to an increase in the value of $k_{App.}$ as depicted

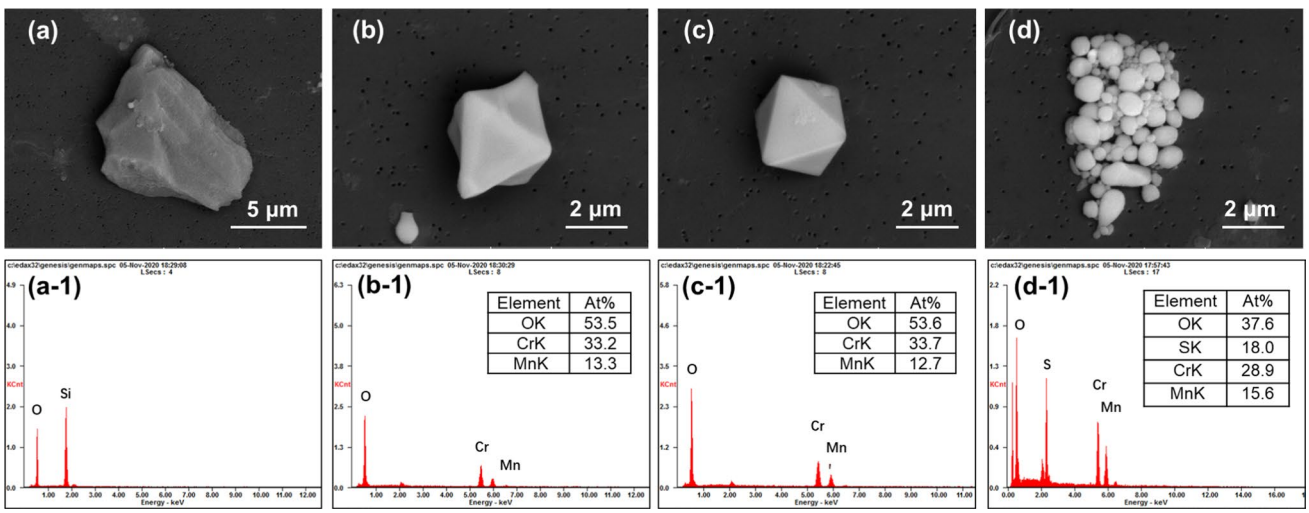

Fig. 5 Morphologies ((**a**) through (**d**)) and corresponding EDS results ((**a-1**) through (**d-1**)) of typical original inclusions in the steel sample before the addition of ladle slag

in Fig. 4a. However, the impact of CaF_2 levels exceeding 10 wt% on $k_{App.}$ was minimal under C/S = 1.7 conditions, as illustrated in Fig. 4b. This suggests that a high-basicity slag with 10 wt% CaF_2 is sufficient for refining Si-killed STS316L.

3.2 Effect of Slag Composition on Evolution Behavior of Inclusions in Si-Killed STS316L

Before the ladle slags were added (reaction time = 0 min), the steel samples contained SiO_2 and MnO · Cr_2O_3 spinel (MC-spinel) inclusions. These morphologies and composition of inclusions are illustrated in Fig. 5. The SiO_2 inclusions had irregular shapes, while the MC-spinel inclusions were octahedral without sulfur and spheroidal with sulfur. The initial SiO_2 inclusions in the steel sample were a result of the silicon deoxidation product.

Figure 6 displays the varying proportions of inclusions in molten steel following the addition of ladle slag with different basicity levels ranging from C/S = 1.0 to 2.3 at 1873 K. The comparison in Fig. 6a, b shows that there is negligible difference in the primary types of inclusions at different time points subsequent to the introduction of S1 (C/S = 1.0) and S2 (C/S = 1.3) slags. However, the quantities of solid particles (such as SiO_2, Al_2O_3 corundum, and MC-spinel) and liquid inclusions exhibit a decrease and increase trend with reaction time, respectively, indicating that the basicity of the slag within the C/S = 1.0–1.3 range minimally influences the types of inclusions in liquid Si-killed STS316L at 1873 K. Figure 7 presents the SEM backscattered electron (BSE) images and EDS findings of inclusions within the steel samples exposed to ladle slags with different basicity levels. The comparison between Figs. 5c, d with Fig. 7c reveals the transformation reaction of original MC-spinel into MnO–Cr_2O_3–SiO_2 inclusions occurring in liquid Si-killed STS316L after the addition of S1 (C/S = 1.0) slag.

Sulfide inclusions (Cr,Mn)S were also identified in the steel samples that interacted with S1 slag after 60 min (Fig. 7d). Oikawa et al. [56] explored the impact of alloying elements on the morphology of (Cr,Mn)S inclusions in Fe–15Cr–0.5Mn–0.3S (wt%) steel. They noted the formation of low-melting point globular (Cr,Mn)S inclusions following a stable monotectic reaction. This response was enhanced by the introduction of C and Si, which reduced the melting point of the iron-rich solution. The occurrence of (Cr,Mn)S inclusions in the steel sample primarily resulted from the low capacity for sulfides in the low basicity slag (S1 slag, C/S = 1.0), leading to adverse effects on the desulfurization process of Si-killed STS316L [51].

With a Vee ratio of C/S = 1.7 (S3 slag), the initial inclusions depicted in Fig. 5 changed to mullite-type inclusions alongside liquid oxides within 5 min after the refractory-slag-metal reaction occurred, as illustrated in Fig. 6a, indicating an increase in the proportion of these inclusions. As the reaction time extended to 60 min, MgO and $MgAl_2O_4$ spinel (MA-spinel) inclusions were visible in Figs. 6b and 7g, h. When the slag basicity was further elevated to C/S = 2.3 (S4 slag), the majority of the initial inclusions were transformed into MgO inclusions, as depicted in Figs. 6b and 7l.

The study utilized the 'Refractory-Slag-Metal-Inclusion (ReSMI)' multiphase reaction model to examine the formation mechanism of inclusion during the interaction of refractory materials, slag, and metal. This model is a modified version of the equilibrium effective reaction zone (EERZ) model [57–59], customized to match the specific experimental conditions as mentioned above in Sect. 2. Through the implementation of the ReSMI model,

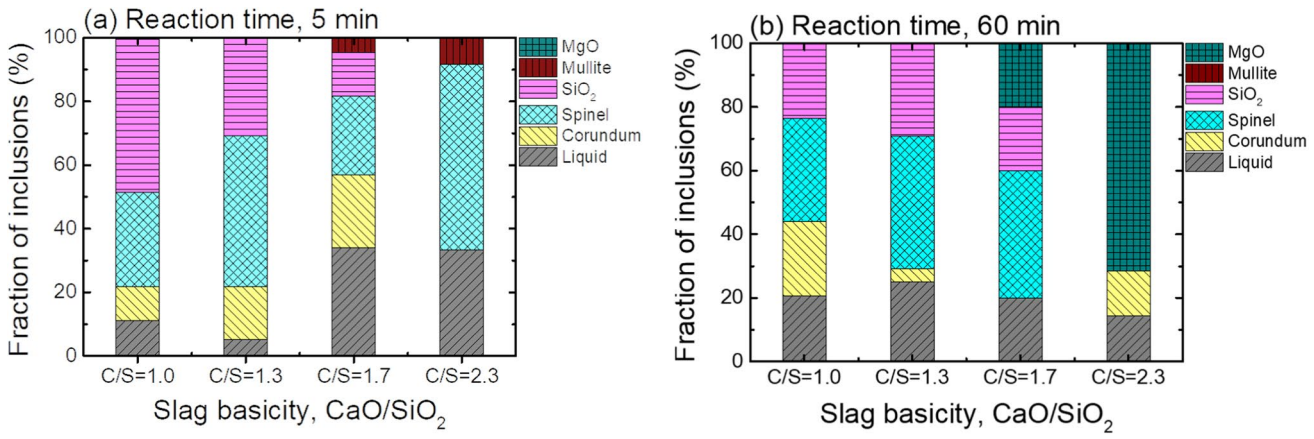

Fig. 6 Varying proportions of inclusions in the liquid steel at (**a**) 5 min and (**b**) 60 min after the addition of the ladle slag with various basicity values from 1.0 to 2.3 at 1873 K

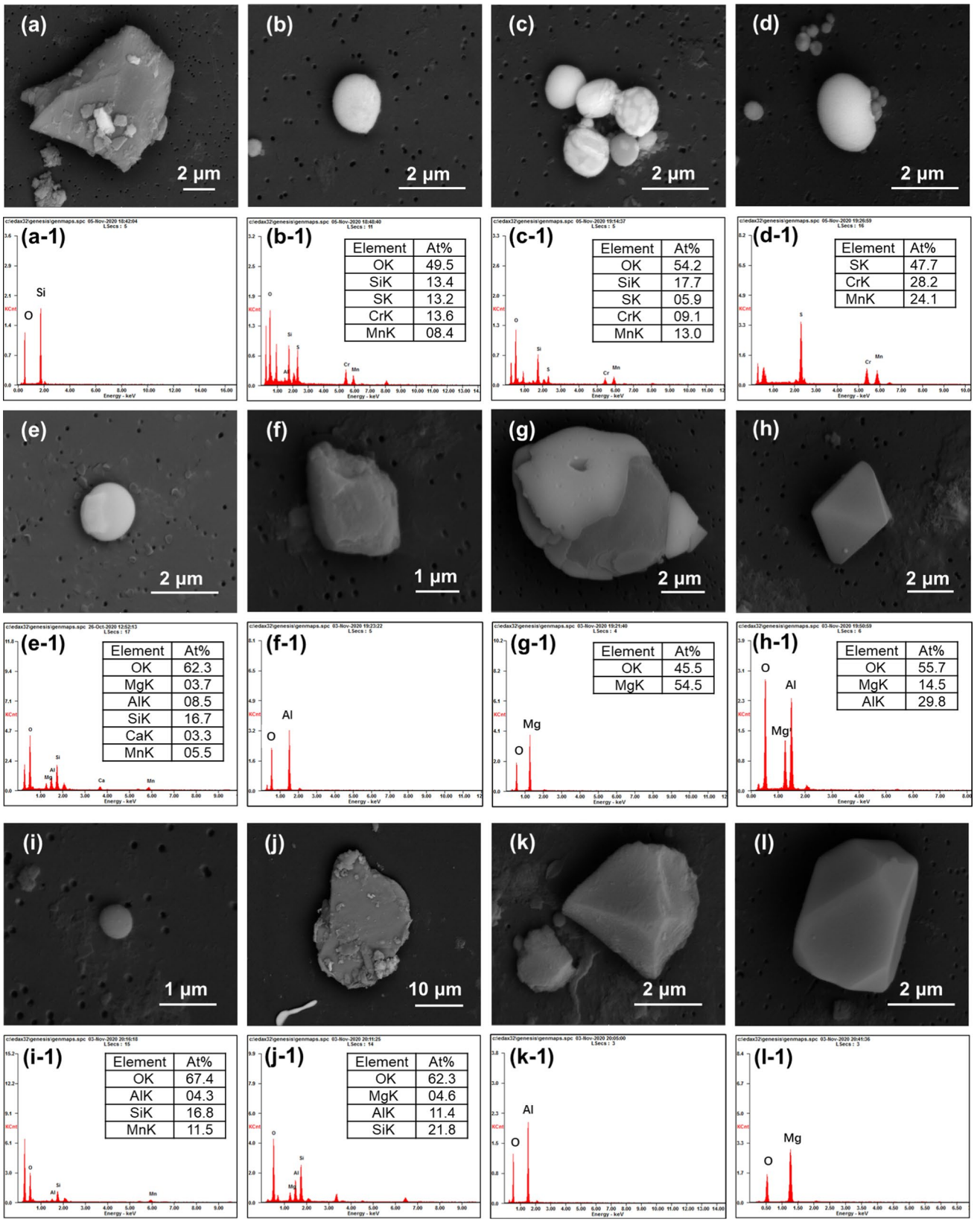

Fig. 7 Morphologies of typical inclusions observed in the steel samples reacted with (**a**) through (**d**) S1 slag, (**e**) through (**h**) S3 slag, and (**i**) through (**l**) S4 slag at 60 min after slags addition (EDS results shown in (#-1) correspond to the oxide inclusions shown in (#))

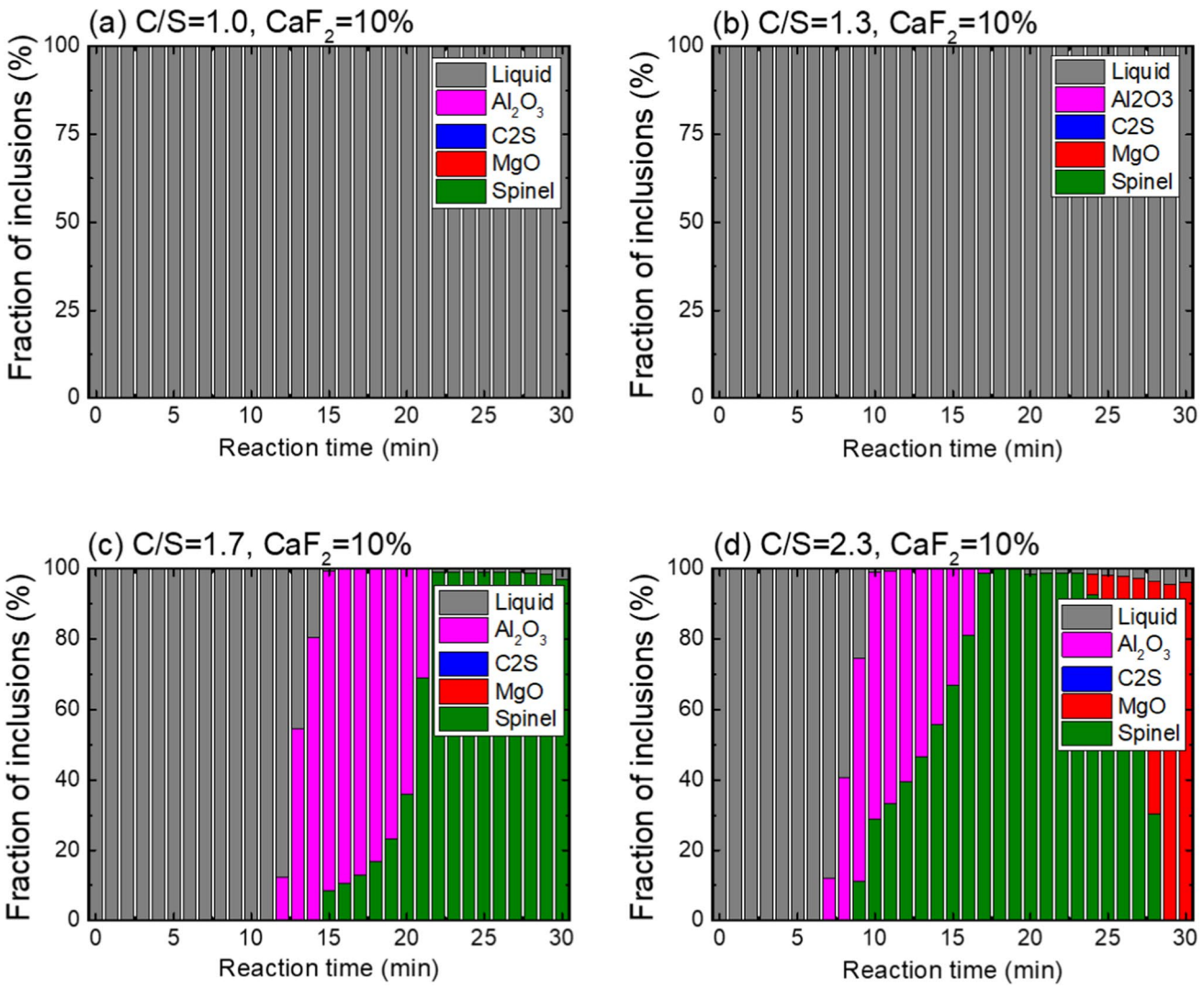

Fig. 8 Evolution of oxide inclusions in the liquid steel reacted with the ladle slag with varied basicity values at a particular CaF_2 concentration (10 wt%) simulated by the ReSMI model at 1873 K: (**a**) C/S = 1.0, (**b**) C/S = 1.3, (**c**) C/S = 1.7, and (**d**) C/S = 2.3

the study successfully predicted changes in the relative fraction and average composition of oxide inclusions over time, as depicted in Fig. 8. Figure 8a, b demonstrated that the introduction of S1 (C/S = 1.0) and S2 (C/S = 1.3) slags into the molten steel at 1873 K could theoretically lead to the formation of liquid inclusions through multiphase reactions. By integrating these findings with the experimental data from Figs. 7b, c, and e, it can be inferred that the presence of liquid oxide inclusions can be classified as MnO–CrO_x–SiO_2 system for S1 slag and MgO–Al_2O_3–SiO_2–CaO system for S3 slag.

Liu et al. [60] and Tanahashi et al. [61] observed a similar trend, reporting that the oxide inclusion composition in liquid STS304 (18Cr–8Ni–0.5Mn–0.05C–Si, wt%) transitioned from MnO–Cr_2O_3 to MnO–Cr_2O_3 + MnO–SiO_2 ([%Si] < 0.7), then to MnO–SiO_2 (0.7 < [%Si] < 2) before reaching equilibrium with the MnO–SiO_2–CrO_x system at 1873 K [61]. The formation of MnO–CrO_x–SiO_2 inclusions is likely due to the reduction of MnO–Cr_2O_3 inclusions by silicon in the melt, as described in Eqs. (4) and (5) [27].

$$2(MnO)_{inclusion} + [Si] = (SiO_2)_{inclusion} + 2[Mn] \quad (4)$$

$$2(Cr_2O_3)_{inclusion} + 3[Si] = 3(SiO_2)_{inclusion} + 4[Mn] \quad (5)$$

Moreover, Ca, Al, and Mg from the liquid slag (Eqs. (6) to (8)) underwent reactions with SiO_2 and/or MnO–Cr_2O_3 inclusions [62–64], leading to elevated levels of CaO, Al_2O_3, SiO_2, and MgO in the inclusions and the generation of the liquid MgO–Al_2O_3–SiO_2–CaO oxide.

$$2(MgO)_{slag} + 3[Si] = 2(SiO_2)_{slag\ or\ inclusion} + 2[Mg] \quad (6)$$

$$2(Al_2O_3)_{slag} + 3[Si] = 3(SiO_2)_{slag\ or\ inclusion} + 4[Al] \quad (7)$$

$$2(CaO)_{slag} + [Si] = (SiO_2)_{slag\ or\ inclusion} + 2[Ca] \quad (8)$$

It can be observed from the preceding discussions that the trend of the calculated results (Fig. 8a, b) closely aligns with the measured results depicted in Fig. 6. Following 60 min of slag additions S1 (C/S = 1.0) and S2 (C/S = 1.3), there is a slight increase in the proportion of liquid inclusions.

When the Vee ratio of the slag was C/S = 1.7 (S3 slag), the formation of blocky Al_2O_3 and octahedral MA-spinel inclusions can be seen in Fig. 7f, h, aligning with the thermodynamic analysis depicted in Fig. 8c. Nishi and Shinme [65] studied the reactions between the Si-Mn killed Fe–42%Ni alloy and the CaO–SiO_2–MgO–Al_2O_3 slag at 1873 K. Their findings indicated an increase in Al_2O_3 content of the original MnO–SiO_2 deoxidation products and a rise in the amount of MgO in MnO–SiO_2–Al_2O_3 inclusions, leading to the formation of MA-spinel inclusions. Park and Todoroki [62] proposed that the higher Al_2O_3 and MgO content in the MnO–SiO_2 deoxidation products may result from the reduction of Al_2O_3 and MgO in ladle slag by Si deoxidizer when the SiO_2 activity in the slag was low. Peng et al. [66] noted that the MgO content in MA-spinel inclusions in 30Cr2Ni4MoV steel dropped with the increase of SiO_2 content in the CaO–SiO_2–MgO–Al_2O_3 ladle slag at 1873 K.

The iso-activity contours of Al_2O_3 and MgO in the ladle slag at 1873 K are shown In Fig. 9. It is revealed that the Al_2O_3 activity in the slag peaked at around $a_{Al_2O_3} \approx 0.01$ at a C/S ratio of 1.7, gradually decreasing with increasing the slag basicity (Fig. 9a). At the same time, the MgO activity in the slag was approximately $a_{MgO} \approx 0.4$ (Fig. 9b). These results suggest that the high activity of Al_2O_3 and MgO, combined with a decrease in SiO_2 activity in the CaO–SiO_2–CaF_2–5%MgO–5%Al_2O_3 slag, facilitates the reduction of Al_2O_3 and MgO in the slag by the Si deoxidizer. This process further promotes the formation of a MA-spinel phase, as demonstrated in Fig. 7h for a slag Vee ratio of C/S = 1.7, as explained in Eqs. (9) and (10) [67].

$$4(Al_2O_3)_{inclusion} + 3[Mg] = 3(MgO \cdot Al_2O_3)_{spinel} + 2[Al] \quad (9)$$

$$(Al_2O_3)_{inclusion} + [Mg] + [O] = (MgO \cdot Al_2O_3)_{spinel} \quad (10)$$

When the ratio of calcium oxide to silica in the slag was 2.3, the appearance of pure MgO inclusions

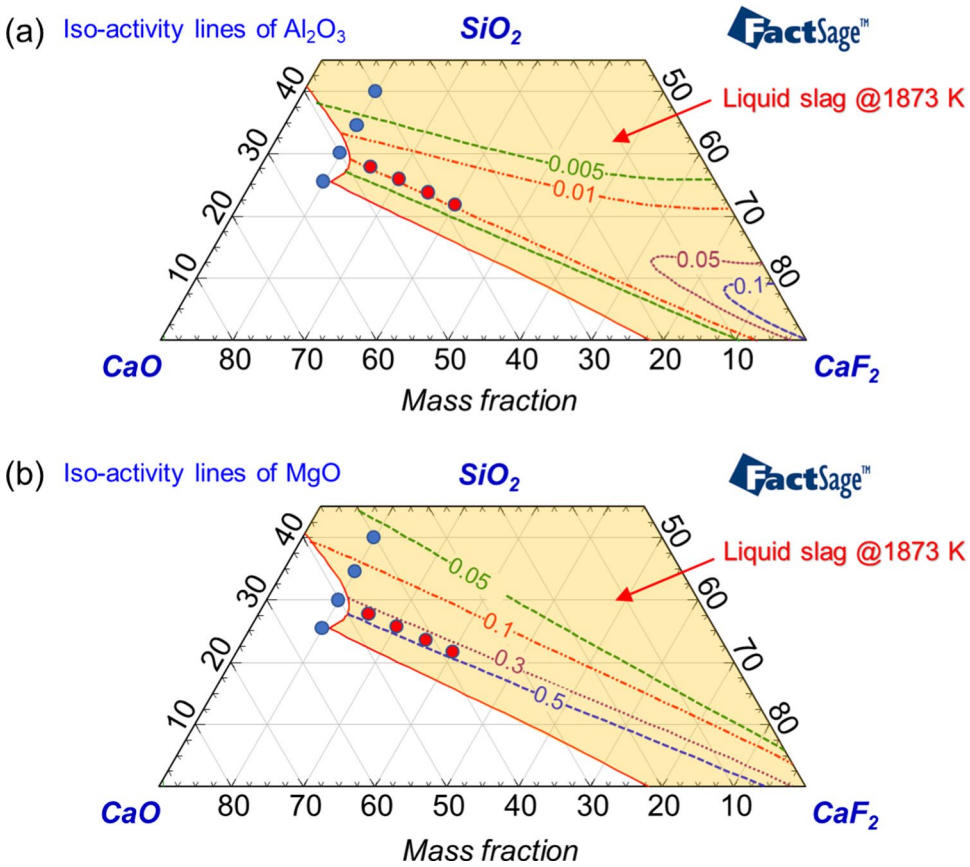

Fig. 9 Calculated iso-activity lines of (**a**) Al_2O_3 and (**b**) MgO in CaO–SiO_2–CaF_2–5%MgO–5%Al_2O_3 slag using FactSage™ 8.2 software at 1873 K

was observed towards the end of the reaction (at 60 min) at a temperature of 1873 K. This occurrence is linked to the MgO activity in the composition of the $CaO–SiO_2–CaF_2–5\%MgO–5\%Al_2O_3$ slag reaching unity, determined using the FactSage™ thermodynamic software [68] and shown in Fig. 9b. Furthermore, the presence of calcium fluoride in the $aO–SiO_2–CaF_2–5\%MgO–5\%Al_2O_3$ slag could hasten the rate at which MgO dissolves from the magnesia crucible into the slag at high temperatures, giving rise to the saturation of the slag by MgO [52, 69]. This led to the suply of Mg from the slag to the molten steel, thereby gradually transforming the MA-spinel inclusions through the incorporation of dissolved Mg into pure MgO oxide inclusions as described by Eq. (11) [70].

$$\left(MgO \cdot Al_2O_3\right)_{spinel} + 3[Mg] = 4(MgO)_{inclusion} + 2[Al] \quad (11)$$

The simulation results presented in Fig. 8c, d confirmed these phenomena. Specifically, the formation of MA-spinel and pure MgO oxide inclusions was observed 15 min and 25 min after the addition of S3 (C/S = 1.7) and S4 slags (C/S = 2.3) respectively. This trend was also reported by Pang et al. [71] and Li et al. [72]. In a study of Zhan et al. [73], the impact of the basicity of refining slag ($CaO–MgO–SiO_2–Al_2O_3–CaF_2$) on inclusions in molten stainless steel (14.5Cr–5.2Ni–0.05C–0.4Si–0.7Mn, wt%) at 1873 K was examined. It was found that the Mg and Al contents increased in the molten steel when reacted with high basicity slag, and the transformation order of oxide inclusions was $Al_2O_3 \rightarrow MgAl_2O_4 \rightarrow MgO$. Liu et al. [74] also noted a rapid transformation time of alumina inclusions into spinel, occurring in just 3 s for alumina inclusions with a diameter of 5 μm. These findings further support that the simulated inclusion composition is consister with the observed results under a slag Vee ratio of C/S = 1.7–2.3.

The results of the macro-simulation shown in Fig. 8c, d indicate that the pure Al_2O_3 inclusion, as seen in Fig. 7f and k, can serve as an intermediate product. It undergoes further reduction by Mg in the molten steel to generate MA-spinel and pure MgO inclusions as described in Eqs. (9) to (11). The occurrence of pure Al_2O_3 inclusions in the liquid steel is likely a result of either the presence of Al from the Si deoxidizer [75] or the higher slag basicity [76–78]. Park et al. [76] conducted thermodynamic equilibrium experiments between the $CaO–SiO_2–MgO–Al_2O_3–CaF_2$ slag and Fe–1.5Mn–0.5Si–0.5Cr (wt%) melts in an alumina crucible at 1873 K. Their study illustrated the Al_2O_3 content in the oxide inclusions increased when slag Vee ratio increased from about C/S = 0.6 to 2.0.

Ren et al. [44] studied the impact of $CaO–SiO_2–MgO–Al_2O_3–MnO–CaF_2$ slag composition on inclusions in Si-killed STS304 at 1873 K. According to their results, they found that the concentration of soluble Al in the liquid steel remained relatively constant as the slag Vee ratio shifted from C/S = 1.0 to 1.8, but notably increased when the ratio increased from C/S = 1.8 to 2.3. This led to the generation of Al_2O_3-rich inclusions in the molten steel, hampering the deformability of these inclusions. Consequently, a higher slag basicity (i.e., increased Al_2O_3 activity in the slag in equilibrium with the Si-killed molten steel, as illustrated in Fig. 9a) results in a greater Al_2O_3 content in the oxide inclusions.

Figure 10 illustrates the simulated results in the average composition of inclusions in molten steel when reacting with slag of different basicity levels at fixed CaF_2 concentration of 10 wt%. Within 30 min of adding S1 (with C/S = 1.0) and S2 (with C/S = 1.3) slags at a temperature of 1873 K, there was a noticeable decrease in Cr_2O_3 and MnO contents, alongside an increase in MgO, Al_2O_3, and CaO contents in the inclusions, as depicted in Fig. 10a, b. This is due to the progress of the abovementioned multiphase reactions Eqs. (4) through (8). With C/S = 1.7 (S3 slag) shown in Fig. 10c, the liquid $MnO–Cr_2O_3–SiO_2$ inclusion transformed to Al_2O_3-rich inclusion after 15 min and followed by the formation of MA-spinel inclusion. Upon further increasing the slag Vee ratio to C/S = 2.3 (S4 slag), the Al_2O_3-rich inclusions transformed into pure MgO inclusions. This transformation is attributed to the saturation of the $CaO–SiO_2–CaF_2–MgO–Al_2O_3$ slag with MgO, resulting in the unity activity of MgO, as shown in Fig. 9b.

According to the results obtained from the ReSMI model, the precipitation of MA-spinel inclusion in the liquid steel occurs when it reacted with slags containing varying CaF_2 contents (ranging from 10 to 30 wt%) at a C/S ratio of 1.7, as illustrated in Figs. 10c and Fig. 11. This is due to the minimal impact of changing CaF_2 levels in the $CaO–SiO_2–CaF_2–5\%MgO–5\%Al_2O_3$ slag on the activities of MgO and Al_2O_3 at 1873 K, as demonstrated in Fig. 9.

Zaitsev et al. [79, 80] reported that adding CaF_2 to the $CaO–Al_2O_3–CaF_2$ slag system did not significantly alter the activities of CaO and Al_2O_3. It is known that slag melts containing fluoride are easily vaporized at high temperatures [81–83]. Consequently, the increase in CaO content due to the decomposition of CaF_2 in the $CaO–SiO_2–CaF_2–5\%MgO–5\%Al_2O_3$ slag may enhance the slag basicity, leading to higher activities of MgO in the liquid slag. This, in turn, could result in the formation of MA-spinel inclusions that, when reacting with Mg, produce pure MgO inclusions.

On the other hand, the deterioration of MgO refractory becomes more severe when exposed to high-CaF_2 slags [52, 84]. This accelerates the migration of Mg from the slag or refractory to the liquid steel, promoting the formation of pure MgO inclusions as described in Eq. (11). The typical

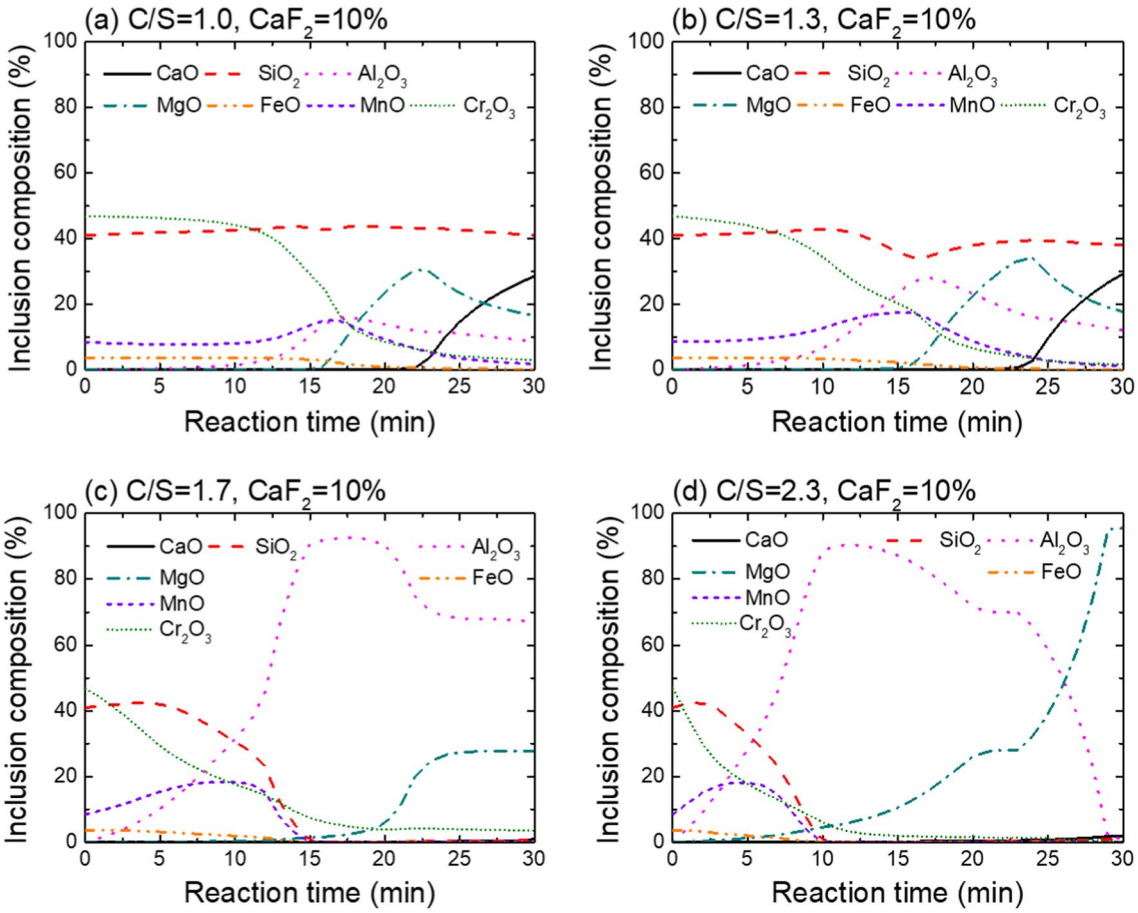

Fig. 10 The variation in the average inclusion composition in the liquid steel reacted with the ladle slag at a given 10% CaF_2 content at 1873 K with different basicity values (**a**) C/S = 1.0, (**b**) C/S = 1.3, (**c**) C/S = 1.7, and (**d**) C/S = 2.3 was obtained using the ReSMI model

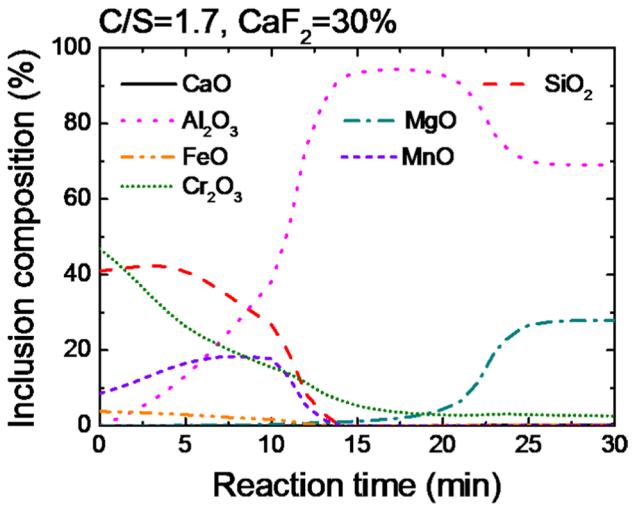

Fig. 11 Results for the variation in average inclusion composition when the liquid steel reacted with the ladle slag at 1873 K were calculated using the ReSMI model under conditions of C/S = 1.7 and CaF_2 = 30%

morphologies of MgO inclusions in liquid steel interacting with a slag containing 30 wt% CaF_2 are depicted in Fig. 12d. Similarly, the presence of liquid MnO–SiO_2–Al_2O_3 system inclusions in Fig. 12a, b, and pure Al_2O_3 in Fig. 12c, are also confirmed in Fig. 11. Deng et al. [67] highlighted that MgO is more vulnerable to reduction by alloying elements in liquid steel compared to CaO in slag under similar conditions due to its near unity activity value, multiple sources (ladle slag and refractory), and greater contact surface area.

4 Conclusions

The impacts of various slag binary basicities (C/S ratio) and CaF_2 contents on the evolution behavior of inclusions in liquid steel was studied by conducting reactions between Si-killed STS316L and CaO–SiO_2–CaF_2–5%MgO–5%Al_2O_3 slag in a MgO crucible at 1873 K. Meanwhile, the evolution of inclusions in molten steel was simulated using the ReSMI thermodynamic model under the same experimental conditions. The key findings are listed as follows:

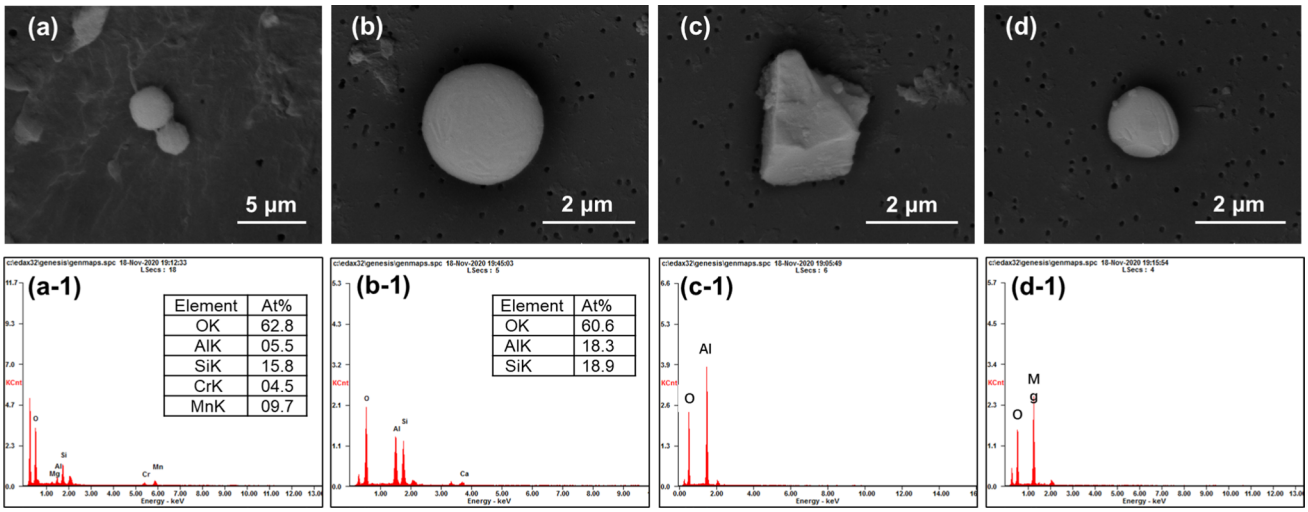

Fig. 12 Morphologies ((**a**) through (**d**)) and corresponding EDS results ((**a-1**) through (**d-1**)) of typical original inclusions in the liquid steel reacted with S8 slag (C/S = 1.7, CaF_2 = 30%) at 1873 K

(1) As the basicity increased from C/S = 1.0 to 2.3 within 30 min after the slag addition, The T.[O] content in the molten steel rapidly decreased. The change in CaF_2 content from 10 to 30% in the relatively basic slag has little influence on the deoxidation of the molten slag at a given slag basicity (C/S = 1.7), indicating that the deoxidation of the liquid steel depends weakly on CaF_2 concentration in the studied slag at 1873 K.

(2) The primary types of initial oxide inclusions in the stainless steel before interacting with the slag are MnO–Cr_2O_3 (MC)-spinel phases. When a slag with relatively low basicity ($CaO/SiO_2 < 1.4$) is added, the formation of liquid MnO–CrO_x–SiO_2 and MgO–Al_2O_3–SiO_2–CaO inclusions takes place. Following the addition of slag with relatively high basicity ($CaO/SiO_2 > 1.6$), the creation of $MgAl_2O_4$ (MA)-spinel inclusions and pure MgO occurs when the slag basicity C/S = 1.7 and 2.3, respectively, at 1873 K.

(3) The pure Al_2O_3 inclusions can act as an intermediate product for the formation of the MA-spinel phase when the slag basicity C/S = 1.7 at 1873 K, which is because the MgO activity increases with the increase of slag binary basicity. When the slag binary basicity increases to C/S = 2.3, the MA-spinel inclusion further reacts with Mg supplied from the slag or refractory to generate MgO inclusions.

(4) The simulated results for the evolution of inclusions under each slag condition are qualitatively in good correspondence with the observed results. The basicity is more dominant factor affecting the evolution of inclusions in STS316L, whereas the CaF_2 is less effective on the variation of inclusions chemistry at relatively basic composition such as C/S = 1.7.

Acknowledgements This work was partly supported by the Korea Evaluation Institute of Industrial Technology (KEIT, Grant Number 20009956) and by the Korea Institute for Advancement of Technology (KIAT, Grant number P0023676, HRD Program for Industrial Innovation), funded by the Ministry of Trade, Industry and Energy (MOTIE), Korea.

Declarations

Conflict of Interest The authors declare that they have no conflict of interest.

References

1. X.H. Chen, J. Lu, L. Lu, K. Lu, Scr. Mater. **52**, 1039–1044 (2005). https://doi.org/10.1016/j.scriptamat.2005.01.023
2. H. Ueno, K. Kakihata, Y. Kaneko, S. Hashimoto, A. Vinogradov, Acta Mater. **59**, 7060–7069 (2011). https://doi.org/10.1016/j.actamat.2011.07.061
3. C. Wang, P. Zhu, F. Wang, Y.H. Lu, T. Shoji, Corros. Sci. **206**, 110549 (2022). https://doi.org/10.1016/j.corsci.2022.110549
4. H.H. Jin, I.S. Ryu, Korean J. Met. Mater. **61**, 137–143 (2023). https://doi.org/10.3365/kjmm.2023.61.2.137
5. J.S. Park, D.M. Cho, S.G. Hong, T.H. Yun, S.J. Kim, Korean J. Met. Mater. **61**, 404–413 (2023). https://doi.org/10.3365/kjmm.2023.61.6.404
6. C. Cho, S. Nam, S. Yu, M. Choi, N. Kang, Korean J. Met. Mater. **60**, 673–684 (2022). https://doi.org/10.3365/kjmm.2022.60.9.673
7. X. He, B.B. He, Met. Mater. Int. **30**, 25–38 (2024). https://doi.org/10.1007/s12540-023-01478-8
8. X. He, X.K. Shang, B.B. He, Met. Mater. Int. **30**, 735–744 (2024). https://doi.org/10.1007/s12540-023-01539-y
9. M. Rostami, R. Miresmaeili, A. Heydari Astaraee, Met. Mater. Int. **29**, 948–967 (2023). https://doi.org/10.1007/s12540-022-01286-6
10. B.H. Reis, W.V. Bielefeldt, A.C.F. Vilela, J. Mater. Res. Technol. **3**, 179–185 (2014). https://doi.org/10.1016/j.jmrt.2014.03.011
11. L. Zhang, B.G. Thomas, ISIJ Int. **43**, 271–291 (2003). https://doi.org/10.2355/isijinternational.43.271

12. W.E. Anable, R.H. Nafziger, D.C. Robinson, JOM **25**, 55–61 (1973). https://doi.org/10.1007/BF03355840
13. D.R. Eo, S.H. Park, J.W. Cho, Mater. Des. **155**, 212–219 (2018). https://doi.org/10.1016/j.matdes.2018.06.001
14. V.B. Vukkum, R.K. Gupta, Mater. Des. **221**, 110874 (2022). https://doi.org/10.1016/j.matdes.2022.110874
15. Q. Chao, V. Cruz, S. Thomas, N. Birbilis, P. Collins, A. Taylor, P.D. Hodgson, D. Fabijanic, Scr. Mater. **141**, 94–98 (2017). https://doi.org/10.1016/j.scriptamat.2017.07.037
16. D. Kong, C. Dong, X. Ni, L. Zhang, J. Yao, C. Man, X. Cheng, K. Xiao, X. Li, J. Mater. Sci. Technol. **35**, 1499–1507 (2019). https://doi.org/10.1016/j.jmst.2019.03.003
17. G. Wang, Q. Liu, H. Rao, H. Liu, C. Qiu, J. Alloys Compd. **831**, 154815 (2020). https://doi.org/10.1016/j.jallcom.2020.154815
18. Y. Zhong, L. Liu, S. Wikman, D. Cui, Z. Shen, J. Nucl. Mater. **470**, 170–178 (2016). https://doi.org/10.1016/j.jnucmat.2015.12.034
19. T. Kurzynowski, K. Gruber, W. Stopyra, B. Kuźnicka, E. Chlebus, Mater. Sci. Eng. A **718**, 64–73 (2018). https://doi.org/10.1016/j.msea.2018.01.103
20. Y.M. Wang, T. Voisin, J.T. McKeown, J. Ye, N.P. Calta, Z. Li, Z. Zeng, Y. Zhang, W. Chen, T.T. Roehling, R.T. Ott, M.K. Santala, P.J. Depond, M.J. Matthews, A.V. Hamza, T. Zhu, Nat. Mater. **17**, 63–71 (2018). https://doi.org/10.1038/nmat5021
21. D. You, S.K. Michelic, C. Bernhard, Steel Res. Int. **91**, 2000045 (2020). https://doi.org/10.1002/srin.202000045
22. B. Coletti, B. Gommers, C. Vercruyssen, B. Blanpain, P. Wollants, F. Haers, Ironmak. Steelmak. **30**, 101–105 (2013). https://doi.org/10.1179/030192303225001694
23. S.I. Chung, Y.H. Shin, J.K. Yoon, ISIJ Int. **32**, 1287–1296 (1992). https://doi.org/10.2355/isijinternational.32.1287
24. M.Y. Zhu, T. Inomoto, I. Sawada, T.C. Hsiao, ISIJ Int. **35**, 472–479 (1995). https://doi.org/10.2355/isijinternational.35.472
25. K. Sakata, ISIJ Int. **46**, 1795–1799 (2006). https://doi.org/10.2355/isijinternational.46.1795
26. X. Yin, Y.H. Sun, Y.D. Yang, X.F. Bai, X.X. Deng, M. Barati, A. McLean, Ironmak. Steelmak. **43**, 533–540 (2016). https://doi.org/10.1080/03019233.2015.1125599
27. J.H. Park, Mater. Sci. Eng. A **472**, 43–51 (2008). https://doi.org/10.1016/j.msea.2007.03.011
28. P.G. Jönsson, L. Jonsson, D. Sichen, ISIJ Int. **37**, 484–491 (1997). https://doi.org/10.2355/isijinternational.37.484
29. C. Liu, F. Huang, X. Wang, Metall. Mater. Trans. B **47**, 999–1009 (2016). https://doi.org/10.1007/s11663-016-0592-2
30. J.S. Park, J.H. Park, Metall. Mater. Trans. B **47**, 3225–3230 (2016). https://doi.org/10.1007/s11663-016-0789-4
31. Y. Li, C. Chen, Z. Jiang, M. Sun, H. Hu, H. Li, ISIJ Int. **58**, 1232–1241 (2018). https://doi.org/10.2355/isijinternational.ISIJINT-2018-048
32. J.H. Shin, J.H. Park, ISIJ Int. **58**, 88–97 (2018). https://doi.org/10.2355/isijinternational.ISIJINT-2017-456
33. J. Guo, S. Han, X. Chen, H. Guo, Y. Yan, Metall. Mater. Trans. B **51**, 1813–1823 (2020). https://doi.org/10.1007/s11663-020-01862-4
34. S.H. Chen, M. Jiang, X.F. He, X.H. Wang, Int. J. Miner. Metall. Mater. **19**, 490–498 (2012). https://doi.org/10.1007/s12613-012-0585-3
35. H. Zhang, Y. Peng, S. Zhang, C. Liu, R. Cheng, H. Ni, Metall. Mater. Trans. B **53**, 702–715 (2022). https://doi.org/10.1007/s11663-021-02420-2
36. J.H. Shin, J.H. Park, Metall. Mater. Trans. B **51**, 1211–1224 (2020). https://doi.org/10.1007/s11663-020-01812-0
37. J.H. Shin, J.H. Park, Metall. Mater. Trans. B **48**, 2820–2825 (2017). https://doi.org/10.1007/s11663-017-1080-z
38. J.H. Shin, Y. Chung, J.H. Park, Metall. Mater. Trans. B **48**, 46–59 (2017). https://doi.org/10.1007/s11663-016-0734-6
39. T.S. Kim, J. Yang, J.H. Park, Metall. Mater. Trans. B **53**, 2523–2533 (2022). https://doi.org/10.1007/s11663-022-02548-9
40. S. Duan, T. Kim, J. Cho, J.H. Park, J. Mater. Res. Technol. **24**, 5165–5176 (2023). https://doi.org/10.1016/j.jmrt.2023.04.115
41. M. Jiang, X. Wang, B. Chen, W. Wang, ISIJ Int. **50**, 95–104 (2010). https://doi.org/10.2355/isijinternational.50.95
42. W.J. Ma, Y.P. Bao, M. Wang, D.W. Zhao, Ironmak. Steelmak. **41**, 26–30 (2013). https://doi.org/10.1179/1743281212y.0000000096
43. Y. Hu, W.Q. Chen, Ironmak. Steelmak. **43**, 340–350 (2016). https://doi.org/10.1179/1743281215y.0000000045
44. Y. Ren, L. Zhang, W. Fang, S. Shao, J. Yang, W. Mao, Metall. Mater. Trans. B **47**, 1024–1034 (2016). https://doi.org/10.1007/s11663-015-0554-0
45. S.C. Duan, X. Shi, M.C. Zhang, B. Li, W.S. Yang, F. Wang, H.J. Guo, J. Guo, Metall. Mater. Trans. B **51**, 353–364 (2020). https://doi.org/10.1007/s11663-019-01729-3
46. E. Andersson, D. Sichen, Steel Res. Int. **80**, 544–551 (2009). https://doi.org/10.2374/sri09sp017
47. L. Zheng, H. Li, X. Wang, Z. Jiang, H. Feng, ISIJ Int. **61**, 1784–1793 (2021). https://doi.org/10.2355/isijinternational.ISIJINT-2020-744
48. M. Valdez, G.S. Shannon, S. Sridhar, ISIJ Int. **46**, 450–457 (2006). https://doi.org/10.2355/isijinternational.46.450
49. Y.M. Gao, S.B. Wang, C. Hong, X.J. Ma, F. Yang, Int. J. Miner. Metall. Mater. **21**, 353–362 (2014). https://doi.org/10.1007/s12613-014-0916-7
50. L. Deng, X. Zhang, M. Zhang, X. Jia, J. Non-Cryst. Solids **500**, 310–316 (2018). https://doi.org/10.1016/j.jnoncrysol.2018.08.018
51. T.S. Jeong, J.H. Cho, J.H. Heo, J.H. Park, J. Mater. Res. Technol. **18**, 2250–2260 (2022). https://doi.org/10.1016/j.jmrt.2022.03.048
52. J.S. Han, J.G. Kang, J.H. Shin, Y. Chung, J.H. Park, Ceram. Int. **44**, 13197–13204 (2018). https://doi.org/10.1016/j.ceramint.2018.04.145
53. J.H. Park, D.J. Min, ISIJ Int. **47**, 1368–1369 (2007). https://doi.org/10.2355/isijinternational.47.1368
54. G.H. Zhang, K.C. Chou, Ironmak. Steelmak. **40**, 376–380 (2013). https://doi.org/10.1179/1743281212Y.0000000055
55. J.H. Park, D.J. Min, H.S. Song, ISIJ Int. **42**, 344–351 (2002). https://doi.org/10.2355/isijinternational.42.344
56. K. Oikawa, S.I. Sumi, K. Ishida, J. Phase Equilib. **20**, 215–223 (1999). https://doi.org/10.1361/105497199770335749
57. M.A. Van Ende, I.H. Jung, ISIJ Int. **54**, 489–495 (2014). https://doi.org/10.2355/isijinternational.54.489
58. M.A. Van Ende, I.H. Jung, Metall. Mater. Trans. B **48**, 28–36 (2016). https://doi.org/10.1007/s11663-016-0698-6
59. M.A. van Ende, Y.M. Kim, M.K. Cho, J. Choi, I.H. Jung, Metall. Mater. Trans. B **42**, 477–489 (2011). https://doi.org/10.1007/s11663-011-9495-4
60. C.S. Liu, W. Liu, H. Zhang, H.W. Ni, J. Iron Steel Res. Int. **30**, 795–807 (2023). https://doi.org/10.1007/s42243-022-00840-1
61. M. Tanahashi, T. Taniguchi, T. Kayukawa, C. Yamauchi, T. Fujisawa, Tetsu-to-Hagane **89**, 1183–1190 (2003). https://doi.org/10.2355/tetsutohagane1955.89.12_1183
62. J.H. Park, H. Todoroki, ISIJ Int. **50**, 1333–1346 (2010). https://doi.org/10.2355/isijinternational.50.1333
63. J. Xu, K. Wang, Y. Wang, Z. Qu, X. Tu, X. Meng, Ironmak. Steelmak. **48**, 127–132 (2021). https://doi.org/10.1080/03019233.2020.1740871
64. L.Y. Li, G.G. Cheng, B. Hu, C.S. Wang, G.Y. Qian, High Temp. Mater. Processes **37**, 521–529 (2018). https://doi.org/10.1515/htmp-2016-0188
65. T. Nishi, K. Shinme, Tetsu-to-Hagane **84**, 97–102 (1998). https://doi.org/10.2355/tetsutohagane1955.84.2_97
66. Y.B. Peng, C.S. Liu, L. Yang, S.W. Hou, R.J. Cheng, H. Zhang, H.W. Ni, J. Iron. Steel Res. Int. **29**, 1434–1445 (2022). https://doi.org/10.1007/s42243-022-00757-9

67. Z. Deng, Z. Liu, M. Zhu, L. Huo, ISIJ Int. **61**, 1–15 (2021). https://doi.org/10.2355/isijinternational.ISIJINT-2020-352
68. I.H. Jung, M.A. Van Ende, Metall. Mater. Trans. B **51**, 1851–1874 (2020). https://doi.org/10.1007/s11663-020-01908-7
69. J.H. Park, D.S. Kim, Metall. Mater. Trans. B **36**, 495–502 (2005). https://doi.org/10.1007/s11663-005-0041-0
70. K. Okumoto, K. Kato, H. Ono, Y. Higuchi, ISIJ Int. **61**, 2370–2380 (2021). https://doi.org/10.2355/isijinternational.ISIJINT-2020-737
71. Z. Pang, R. Zhu, P. Chen, Z. Wang, Metall. Res. Technol. **114**, 211 (2017). https://doi.org/10.1051/metal/2017028
72. Y.Y. Li, W. Yang, L.F. Zhang, Metals **10**, 444 (2020). https://doi.org/10.3390/met10040444
73. Z. Zhan, Y. Zhang, R. Shi, T. Qiao, G. Wang, G. Cheng, Metals **13**, 750 (2023). https://doi.org/10.3390/met13040750
74. C. Liu, M. Yagi, X. Gao, S.J. Kim, F. Huang, S. Ueda, S. Kitamura, Metall. Mater. Trans. B **49**, 113–122 (2018). https://doi.org/10.1007/s11663-017-1122-6
75. J.H. Park, Y.B. Kang, Metall. Mater. Trans. B **37**, 791–797 (2006). https://doi.org/10.1007/s11663-006-0061-4
76. J.S. Park, J.H. Park, Metall. Mater. Trans. B **45**, 953–960 (2013). https://doi.org/10.1007/s11663-013-9998-2
77. H. Yang, J. Ye, X. Wu, Y. Peng, Y. Fang, X. Zhao, Metall. Mater. Trans. B **47**, 1435–1444 (2016). https://doi.org/10.1007/s11663-015-0581-x
78. J.W. Kim, S.K. Kim, D.S. Kim, Y.D. Lee, P.K. Yang, ISIJ Int. **36**, S140–S143 (1996). https://doi.org/10.2355/isijinternational.36.Suppl_S140
79. A.I. Zaitsev, N.V. Korolyov, B.M. Mogutnov, J. Chem. Thermodyn. **22**, 513–530 (1990). https://doi.org/10.1016/0021-9614(90)90144-F
80. A.I. Zaitsev, N.V. Korolyov, B.M. Mogutnov, J. Chem. Thermodyn. **22**, 531–543 (1990). https://doi.org/10.1016/0021-9614(90)90145-G
81. S.C. Duan, H.J. Guo, Steel Res. Int. **91**, 1900634 (2020). https://doi.org/10.1002/srin.201900634
82. J.H. Park, D.J. Min, Steel Res. Int. **75**, 807–811 (2004). https://doi.org/10.1002/srin.200405846
83. C.B. Shi, J. Li, J.W. Cho, F. Jiang, I.H. Jung, Metall. Mater. Trans. B **46**, 2110–2120 (2015). https://doi.org/10.1007/s11663-015-0402-2
84. J.H. Shin, J.H. Park, J. Iron. Steel Res. Int. **25**, 157–163 (2018). https://doi.org/10.1007/s42243-018-0014-6